Trans. Indian Inst. Met.
Vol.60, No.5, October 2007, pp. 487-494

TP 2167

Stress-Strain Properties of Ferritic Steels using Automated Ball-Indentation Testing – Pile-up Effects Included

V. Karthik, K.V. Kasiviswanathan, A. Vijayaragavan, K. Laha and Baldev Raj
Metallurgy and Materials Group, Indira Gandhi Centre for Atomic Research, Kalpakkam
Email: karthik@igcar.gov.in
(Received 09 October 2006 ; in revised form 21 June 2007)

ABSTRACT

The automated Ball-Indentation (BI) testing is based on repeated indentation of a spherical indenter at a single location on a metallic sample. The indentation loads and the corresponding depths in an indentation are used to extract the key mechanical flow properties using well established mathematical relationships. The technique is almost non-destructive and an excellent substitute for the conventional tensile test especially when there is very little volume of specimen available for testing. The distortion at the original plane of surface caused by the material displaced by the indentation is referred to as the pile-up or sink-in effect. The pile-up behaviour alters the actual contact area and hence the indentation diameter which is used for calculating the stress-strain parameters. It is well established that the extent of pile-up is related to the strain hardening coefficient of the material. This paper describes the methodology for deriving the plastic stress-strain properties by automated ball-indentation technique taking into account the usually ignored pile-up effects. Flow properties derived from ball-indentation tests using the proposed methodology were found to be in good agreement with those of tensile test results for various ferritic steels like AISI 1025 carbon steel, 2.25Cr-1Mo steel, Mod 9Cr-1Mo steel with different work hardening characteristics.

Keywords: Spherical indentation, pile-up, strain hardening, ferritic steels, stress-strain

1. INTRODUCTION

The evaluation of mechanical properties of structural components is very essential for their continued safe operation. When this assessment is done without disturbing the structural integrity and functional capabilities of the plant components, the economic benefits reaped are enormous. This demands techniques that require minimum sampling volume and that are simple, non-destructive and suitable for localized zones. One such technique is the Ball-Indentation (BI) testing technique. The BI test is based on repeated indentation of a spherical indenter at a single location on a metallic sample. The indentation loads and the corresponding depths are used to find out key mechanical properties using well established mathematical relationships[1]. The BI technique is an excellent substitute for the conventional tensile tests especially when there is very little volume of material available for testing like in the case of weldments[2], failed components and in alloy development applications[3]. The use of in-situ BI tests for remaining life assessment of plant components is also gaining popularity[4].

2. ABOUT THE TEST TECHNIQUE

Hardness tests are widely used to provide a quick measure of the flow stress of the material. Numerous investigators have developed alloy specific hardness-strength relationships which are mostly empirical in nature. Hardness tests using spherical indenters (like Brinell hardness) are unique because the geometry of indentation changes with increasing penetration. Consider the indentation of a metal surface by a spherical indenter of diameter D to a depth h_t. This result in a plastic indentation which is a section of the spherical indenter with a chordal diameter d_p (Fig. 1a). The indentation geometry d/h changes with increasing penetration of the indenter. Hence a unique flow stress and a corresponding plastic strain can be associated with particular indentation geometry (d/h). Thus different values of flow stress and plastic strain can be generated for a test material using a series of spherical indentations of different sizes[5]. This is not possible with conical or pyramidal indenters where geometrically similar indentations are produced and the ratio d/h and the flow stress essentially remain constant with increasing penetration of the indenter.

Tabor[1] demonstrated that the mean pressure H developed between the spherical indenter and the test material increases with increasing load and can be related to the flow stress of the material as

$$H = \Psi\sigma \qquad (1)$$

Where $H = 4P / \pi d_p^2$
P = Indentation load
Ψ = Constraint factor
σ = Flow stress

For spherical indentation, the growth of the indentation geometry with increasing load occurs in three stages: (i) The elastic regime[6], where the deformation is reversible and is described by Hertz Contact solution with Ψ having a constant value of 1.1 (ii) The transition regime, starting with the initiation of plastic zone beneath the indenter, where the ratio H/σ increases with d_p and (iii) The fully plastic regime in

which the plastic zone expands to the surface of the specimen and the contact pressure increases due to work hardening characteristics and Ψ attains a constant value. This increase in the mean contact pressure with the increasing penetration in the transition and fully plastic regimes makes it possible to derive the plastic flow properties of the material. Different values can be obtained from the literature for the parameter ψ during the three stages of the indentation process [6,7]. Francis statistically analyzed the published experimental data and obtained a value Ψ = 2.87 in the fully plastic regime.

The strain in spherical indentation is maximum just below the center of the region of contact and reduces with radial distance from the axis of symmetry to about 20% of the maximum value at the periphery of indentation. The average strain beneath the indenter has been defined in various ways. Tabor[1] showed that

$$\varepsilon_p = 0.2\ d_p / D \qquad (2)$$

Since the maximum strain that can be obtained from above equation is 0.2, this equation has the limitation that it cannot be used to describe the flow strain for materials with very large strain or elongation. Various other definitions of average strain in indentation testing have been outlined by Ahn[8]. Of all the strain definitions, Ahn showed that the use of shear strain at the contact edge defined by 0.12tanγ resulted in best agreement between the stress-strain curves derived from ball-indentation and tensile tests for various steels tested. This definition of strain is

$$\varepsilon_p = \frac{\alpha}{\sqrt{1-(a/R)^2}}\frac{a}{R} = \alpha \tan\gamma \qquad (3)$$

where tanγ is the shear strain at the contact edge (Fig. 1b) and α is a material independent constant[9] estimated to be 0.12.

Thus, by performing spherical indentation on a metallic sample with progressively increasing loads at a single location, the flow stress and the corresponding plastic strain can be obtained using the measured values of indentation load (P) and plastic indentation diameter (d_p). The true stress-strain data can then be fitted to suitable constitutive equations like the Hollomon[10], Ludwik or Voce equations to determine the strain hardening coefficient (n) and the UTS.

Several workers[11] have resorted to direct measurement of d by optical techniques. A cyclic ball-indentation test was first developed by Au[12] et al. and then patented as Automated Ball Indentation by Haggag[13]. The ABI, patented by Haggag is based on multiple indentation cycles on a metallic sample at the same location by spherical indenter. Each cycle consists of loading, partial unloading and reloading sequences as shown in Fig. 2. The plastic indentation depth, h_p, after complete removal of load is obtained by extrapolating the partial unloading curve linearly to zero load. The plastic indentation diameter d_p is obtained using the following Hertz's relation.

$$d_p = \{0.5\ CD\ [h_p^2 + (d_p/2)^2] / [\ h_p^2 + (d_p/2)^2 - h_pD]\}^{1/3} \qquad (4)$$

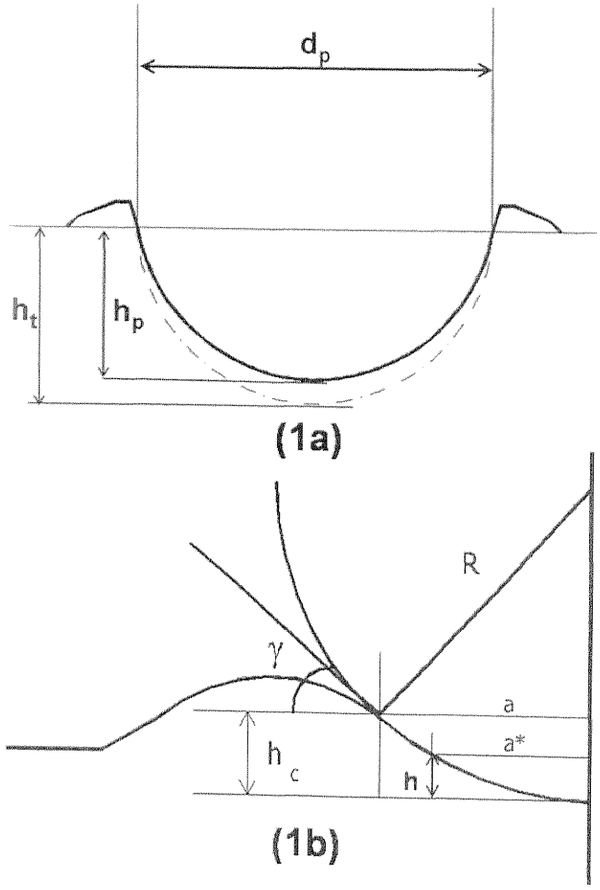

Fig. 1 : Schematic Representation of the spherical indentation geometry

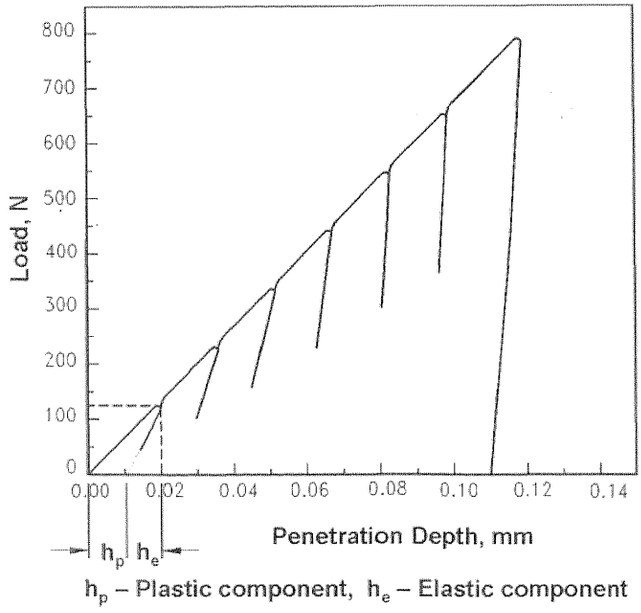

Fig. 2 : Multiple Loading-Unloading curve in a Ball-indentation test

C = 5.47 P $(1/E_I + 1/E_2)$

E_I = Elastic Modulus of the indenter

E_2 = Elastic Modulus of the sample

Having found d_p iteratively using eq. (4), the true stress and plastic strain can be obtained using the eqs. 1 and 2. According to Tabor, eq. 4 which is developed with the assumption of an ideal spherical depression, gives good results for shallow indentations, but a large discrepancy occurs for deeper indentations ($d_p/D \geq 0.7$).

Alternatively, one can analyze the raw load-depth data in an indentation testing in terms of the contact depth 'h' and contact radius 'a'. Considering the load-indentation depth curve shown in Fig. 3, the contact depth h is obtained using the Sneddon's analysis[14].

$$h = h_{max} - \omega\ (h_{max} - h_i) \tag{5}$$

where h_{max} is the maximum indentation depth, h_i is the intercept indentation depth and ω the indenter shape parameter is 0.75 for a spherical indenter. Using the geometrical relationship, the indentation contact diameter is estimated from the indentation contact depth h. (Fig. 1b)

$$d^* = 2a^* = 2\sqrt{h(D - h)} \tag{6}$$

d* is the contact diameter and a* is the contact radius in the plane of original surface.

The raising up/dipping in of the circle of contact relative to the original surface is referred to the pile-up/sink-in phenomenon. The pile-up or sink-in effects during indentation significantly alters the actual contact area and thereby the actual indentation diameter. It may be noted that neither eq. (4) nor eq. (6) accounts for the changes in indentation contact diameter due to pile-up or sink-in effect. Norbury and Samuel[15] measured the contact circle diameter on the recovered indentation and calculated its relative height to the original surface. They found that the ratio of the height of pile-up to penetration depth below the circle of contact i.e. h_{pile}/h_c (Fig 1b) is a material constant and is dependent on 'n', the strain hardening coefficient. Hill[16] et. al also established that the ratio h_{pile}/h_c is a numerical constant dependent only on 'n'. The resulting relationships obtained using non-linear elasticity theory and verified by finite element computations was expressed as

$$c^2 = a^2/hD = h_c/h = 1 + h_{pile}/h = a^2/a^{*2} \tag{7}$$

where 'c' - a numerical invariant

a^* - Contact radius in the plane of original surface (d*/2)

a - Contact radius in the plane of pile up (d/2)

Fitting this invariant 'c' to the experimental data obtained by Norbury and Samuel for a range of materials, Hill proposed the following relationship

$$c^2 = \frac{a^2}{a^{*2}} = \frac{d^2}{d^{*2}} = \frac{5(2-n)}{2(4+n)} \tag{8}$$

$$d^2 = \frac{5(2-n)}{2(4+n)} d^{*2} = \frac{5(2-n)}{2(4+n)}\left(hD - h^2\right) \tag{9}$$

The contact circle lies in the plane of the original surface only when $c^2 = 1$, which marks the boundary between the piling up and sinking in. This corresponds to the strain hardening exponent of about 0.28 which is in close agreement with the experimental value obtained by Norbury and Samuel.

From the eq. (8), it can be inferred that extent of pile-up depends on the work hardening characteristics of the material. If 'n' is very low like in a cold worked material, the large plastic zone beneath the indenter and the surrounding elastic volume are not able to accommodate the volume change due to the indenter penetration and hence pile up occurs. Thus pile-up effects are more prominent in materials with low strain hardening coefficients.

Equation (9) gives the real indentation contact diameter between the indenter and the specimen accounting for the pile-up effects. The actual indentation diameter after each loading-unloading cycle of the load-depth curve can be determined using the eqs. (5), (9) and knowing the value of 'n'. But since the strain hardening coefficient 'n' is an unknown to be determined from stress-strain data of the indentation tests, the following iterative procedure is used in the present work to determine the true stress-strain data. For each loading-unloading cycle, knowing the value of h using eq. (5) and assuming an initial value of n, d is calculated using eq. (9). Then s and ε_p are calculated using eqs. (1) & (3). Fitting the stress-strain data to the appropriate constitutive equation, the value of 'n' is calculated and compared with the initial input value of 'n'. The iteration is continued until the assumed initial value of 'n' equals that calculated.

For the familiar power law Hollomon equation fitting

$$\sigma = K\ (\varepsilon_p)^n \tag{10}$$

'n' is calculated from the slope of the log-log plots of true stress- strain data. This along with the strength coefficient (K) is used to calculate the Ultimate Tensile Strength (σ_{UTS}) using the well known expression

$$\varepsilon_U = n \text{ and } \sigma_{UTS} = K(n/e)^n \tag{11}$$

where ε_U = True Uniform Elongation

e = 2.71

For steels like the 2.25Cr-1Mo and 9Cr-1Mo steels, it has been observed that Voce equation provides a better fit to the flow properties[17].

$$\sigma = K - B \exp(-Ce) \tag{12}$$

The σ_{UTS} and the % true uniform elongation are obtained from the following equations using the fit parameters K, B and C.

$$\varepsilon_U = \ln (B\ (1+C)/K) / C \tag{13}$$

Table 1
Chemical composition of the various alloys used in this study

In% wt	C	Si	Mn	P	S	Cr	Mo	Ni	N	Nb	V	Fe
AISI Type 1025	0.23		0.40	0.040	0.040							Balance
2.25Cr-1Mo steel	0.06	0.18	0.48	0.008	0.008	2.18	0.93					Balance
Mod 9Cr-1Mo steel	0.096	0.32	0.46	0.012	0.006	8.72	0.90	0.1	0.05	0.08	0.22	Balance

Table 2
Summary of various heat treatments on 2.25Cr-1Mo and Mod 9Cr-1Mo steels

Details of Heat-treatment for Mod 2.25Cr-1Mo steel

Heating to a temperature T Kelvin, soaking for 5 min followed by oil quenching and tempering at 1023K/1hr

Sample ID	Temperature T Kelvin	Time t Mins	Hardness HVN
1	1083	5	200
2	1128	5	155
3	1153	5	186
4	1100	1	170
5	1173	1	196
6	1473	1	240

Details of Heat-treatment for 9Cr-1Mo steel

Heating to a temperature T Kelvin, soaking for 5 min followed by oil quenching and tempering at 1023K/1hr

Sample ID	Temperature T Kelvin	Hardness HVN
1.	1073	205
2	1223	213
3	1273	223.5
4	1323	240
5	1423	255.5
6	1573	260
7	1623	252.2

$$\sigma_{UTS}=K-B \exp(-C_U) \quad (14)$$

The stress-strain flow curve, 'n' and σ_{UTS} determined by ball-indentation tests are compared with the corresponding tensile data for validating the test technique.

3. EXPERIMENTAL DETAILS

The aim of the present work is to demonstrate the usefulness of the ball-indentation technique for estimating the uniaxial tensile properties and evolve a methodology for including the effects of pile-up in deriving the stress-strain relationships. The alloys taken up for this study are AISI

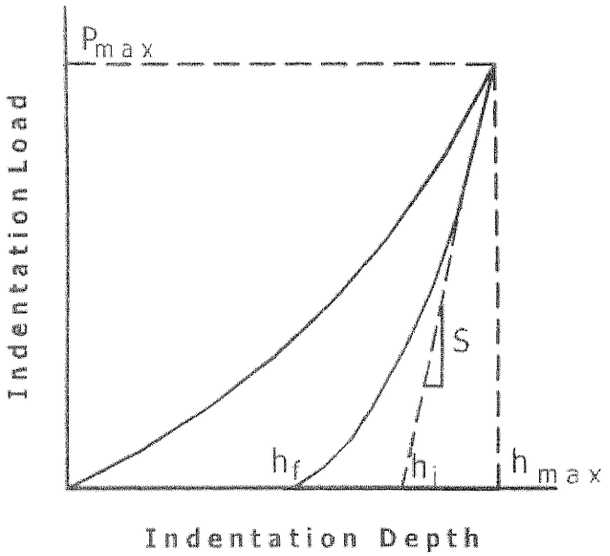

Fig. 3 : Typical parameters of Loading-Unloading curve used for estimating contact depth by Sneddons Analysis

1025 carbon steel, 2.25Cr-1Mo and Mod 9Cr-1Mo steels. Table 1 gives the chemical composition of the material studied. To validate and benchmark the ball-indentation technique for these alloys, a variety of heat treatments, as summarized in Table 2, were carried out on 2.25Cr-1Mo and Mod 9Cr-1Mo ferritic steel alloys to simulate a range of microstructures and mechanical properties. Since pile-up effects are predominant in materials with low strain hardening coefficient 'n', the heat simulations carried out ensured a variety of microstructures with wide range of strain hardening coefficients (n = 0.05 to 0.15).

Both conventional uniaxial tensile tests and ball-indentation tests were performed on these simulated heats to compare, analyze and validate the ball-indentation test technique. Tensile tests were carried out on cylindrical tensile specimens (26-mm gauge length and 4 mm diameter) fabricated from the different heat-treated microstructures at a nominal strain rate of 3×10^{-4} s^{-1} at ambient temperature (298 K) as per ASTM E-8M using a floor model Instron 1195 universal testing machine.

For carrying out automated ball-indentation tests, a miniature mechanical test system was designed and developed at IGCAR. (Fig. 4) The basic test system is a closed loop servo hydraulic test machine consisting of a servo-actuator with an LVDT for its positional inference, a high precision load cell

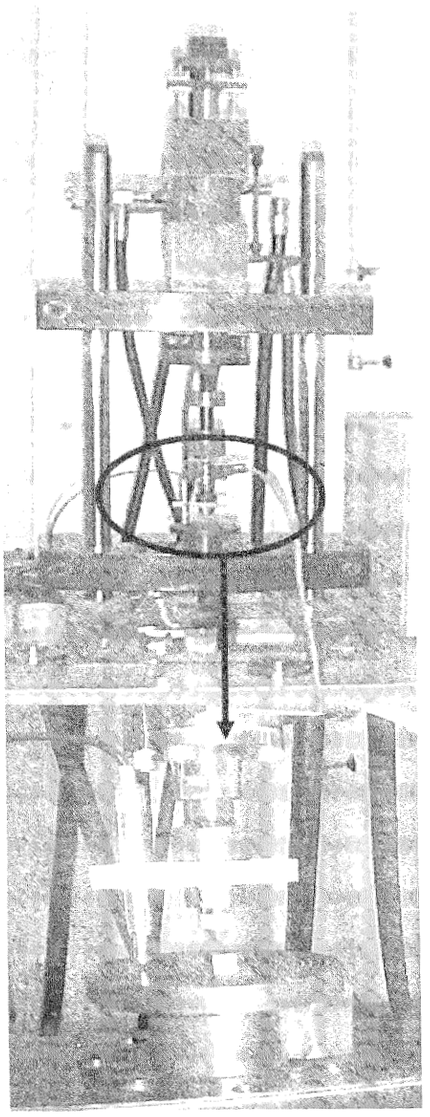

Fig. 4 : The table top servo hydraulic ball-indentation test system developed at IGCAR

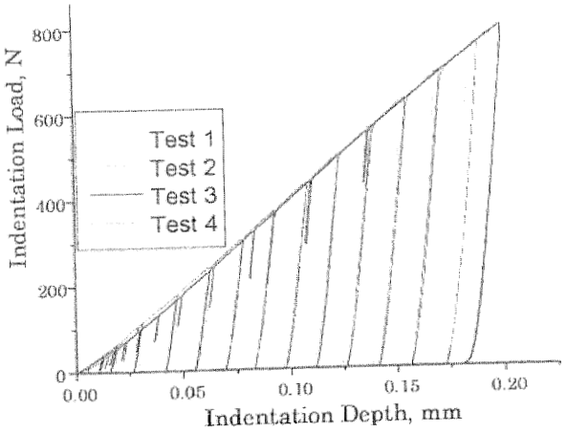

Fig. 5 : Typical indentation load-depth curve of 4 repeatable ball-indentation test performed on AISI 1025 carbon steel

(200 kg capacity, HBM make) as the load sensor and a short stroke LVDT (accuracy - ± 0.5 µm, resolution – 0.1 µm) for precise measurement of the indentation depths. The test system is equipped with a microprocessor based closed loop digital servo controller with provisions for ramping at user defined speeds using a Window based Graphic User Interface (GUI) with real time data acquisition.

Extensive trials were carried out to automate and standardize the ball-indentation test procedure on the servo-hydraulic test system. The test involved performing about 10 to 12 sequential loading-unloading cycles at a single location on the test specimen. The spherical indenter was a tungsten carbide ball of 1 mm or 1.2 mm (± 2.5µm) diameter and indentation testing was performed at a nominal speed of 0.1mm/min. The test procedure was standardized on hardness calibration blocks to get repeatable load-depth plots. The test which is completely automated takes about 5 minutes duration and the raw data obtained is processed using post-processing software involving the mathematical equations described in the previous section.

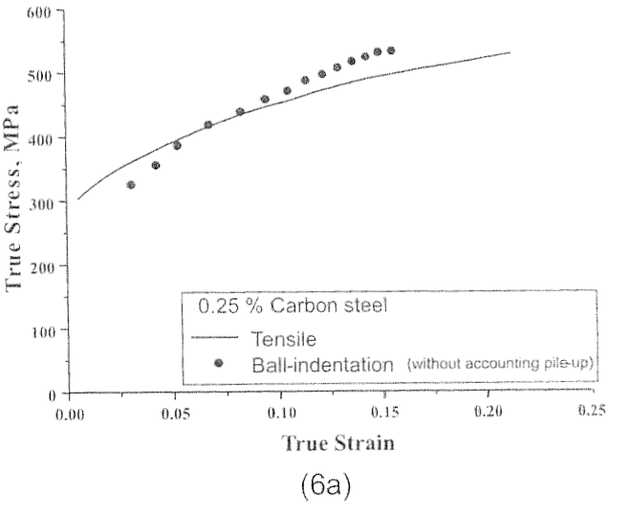

(6a)

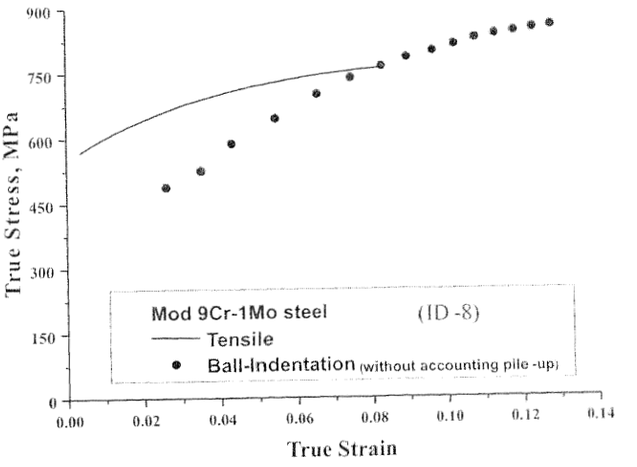

(6b)

Fig. 6 : Stress-Strain plot of BI test without considering pile up effects superimposed on respective tensile stress-strain plots

Ball-Indentation tests were performed at ambient temperature on the various alloys selected in this study. The specimen for indentation testing was 8 mm in diameter and 4 mm thick. Specimens were EDM wire cut and surfaces were finally polished with 1μm diamond paste. More than five indentation tests per specimen were performed to examine the reproducibility. The results of the BI tests performed on various alloys and their comparison with tensile properties is presented in the following section.

4. RESULTS AND DISCUSSION

Figure 5 shows the repeatable indentation load-depth plot of a typical BI test indicating excellent reproducibility with a scatter of less than 2% in load values at any particular depth. The plastic indentation depths for the different loading cycles were first obtained from the unloading cycle using eq. (5) and converted to the indentation diameters using eq. (6). Without considering the pile-up effects, the stress and corresponding strains were calculated using eqs. 1 & 2. The stress-strain data of the AISI 1025 carbon steel was fit to Hollomon power law equation while those of 2.25Cr-1Mo and Mod 9Cr-1Mo steels were fit to Voce equation to determine the UTS and true uniform elongation 'ε_U'.

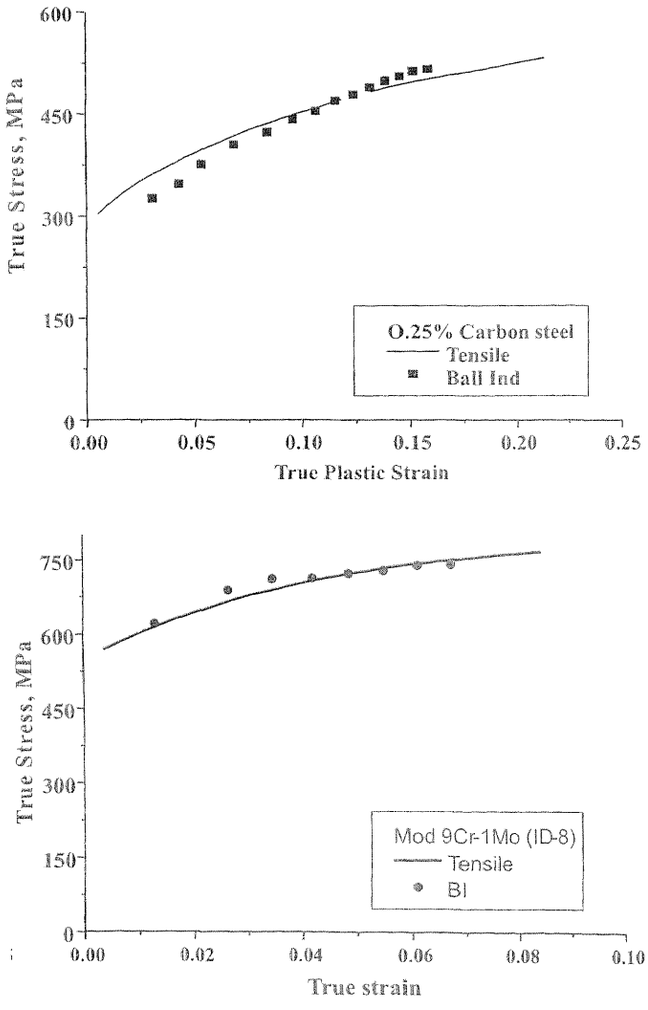

Fig. 7 : Stress-Strain plot of BI test with pile up effects accounted superimposed on corresponding tensile stress-strain plots

Table 3

Comparison of the results of ball-indentation tests and conventional tensile tests for the various ferritic steels.

Material/ID		Tensile test results		Ball-indentation test results	
		UTSMPa	ε_U%	UTSMPa	ε_U%
AISI 1025 carbon steel		432	0.21	455	0.193
2.25Cr-1Mo steel	ID:1	521	0.091	519	0.111
	2	529	0.108	531	0.104
	3	594	0.074	613	0.079
	4	480	0.142	477	0.123
	5	674	0.082	683	0.085
	6	762	0.064	735	0.061
Mod 9Cr-1Mo steel	ID:1	639.36	0.100	640.48	0.085
	2	608.69	0.119	614.32	0.095
	3	702.16	0.083	682.06	0.06
	4	734.28	0.072	736.11	0.074
	5	789.18	0.057	786.2	0.068
	6	803.896	0.054	805.78	0.051
	7	812.98	0.052	830.20	0.058

Figure 6 shows the stress-strain data of BI test superimposed on the tensile test results when the raw data of BI test are analysed without considering the pile-up effects. For the plain carbon steel with n~0.2, a shift of about 10 % in the stress value is noted (Fig. 6a) for a given strain. The higher stress values calculated using equation $\sigma = 4P / \pi d_p^2 C$ is due to lower value of the indentation diameter d_p determined without considering the pile up effects. The pile-up effect alter the indentation contact area and increases the actual indentation contact diameter as shown in Fig. 1b .

But when the stress-strain data of a material with $n \leq 0.10$ is superimposed on the corresponding tensile data, the resulting plot (Fig. 6b) shows both upward and lateral shift from the corresponding tensile plot with respect to both stress and strain values. This lateral shift in the strain to higher values suggests that the empirical relation relationship $\varepsilon_p = 0.2\ d_p/D$ does not truly represent the true strain at the indentation edge for materials with very low n values. FEM analyses of the indentation process done by Taljat[18] et al. has showed that the true plastic strain computed at d/D=0.5 for three different n values of 0.0, 0.25 and 0.5 varied between 0.05 and 0.15 while the value according to equation $\varepsilon_p = 0.2\ d_p/D$ is 0.1. Thus the discrepancies in the ball-indentation results were attributed to the non-inclusion of pile up effects and in the definition of true plastic strain especially for materials with $n < 0.15$.

Alternatively, the measured indentation load-depth curves for the different materials under study were analyzed using eqs. (5) and (6). Considering the equations for pile-up, the corrected indentation diameters and the true stress-strain values are calculated using the iterative method outlined in

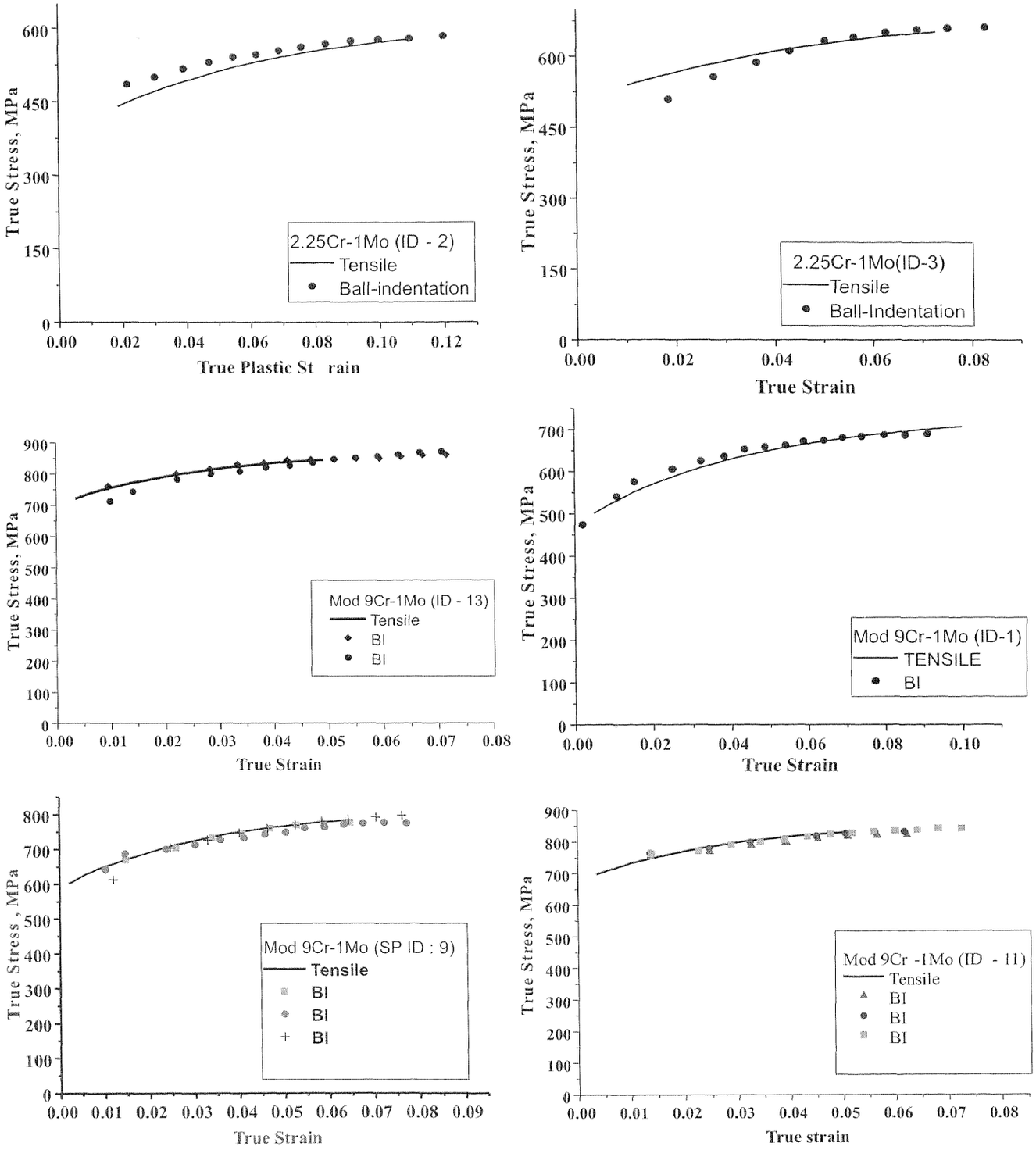

Fig. 8 : Comparison of the stress-strain curves obtained from the ball-indentation tests and conventional tensile tests for the various heat treated microstructures of 2.25Cr-1Mo and Mod 9Cr-1Mo steels

the previous section using the eqs. (9), (1) & (3) and the constants Ψ=2.87 and α = 0.12. Figures 7, 8 and table 3 compares the flow properties obtained from BI test and the conventional tensile stress-strain properties for the various materials under study.

It can be clearly seen that the inclusion of pile-up effects and the strain definition according to eq. (3) results in very good agreement between the stress-strain curve obtained from ball-indentation and those derived from conventional tensile tests. The pile-up or sink-in caused mainly by work hardening characteristics has a strong effect on calculating the absolute values of the stress and strain values. Also the result that a constant value of 2.87 for the constraint factor $\Psi = H/\sigma$ for a range of work hardening exponents in this study matches well with similar studies[7]. The use of new strain definition of

0.12 tanγ instead of commonly used expression 0.2 d_p/D results in good agreement of stress-strain values with the conventional tensile tests especially for steels showing pile-up effects, inline with the work done by Sung-Hoon Kim[9] et al.

Thus a methodology for accurately determining the stress-strain properties for ferritic steels with different work hardening characteristics using ball-indentation technique has been established. The methodology also accounts for the pile-up effects exhibited by these steels. This opens up the usefulness of the technique for a wide variety of applications where little volume of material is only available for extracting the mechanical properties. The ferritic steels like 2.25Cr-1Mo and Mod 9Cr-1Mo steels are widely used as high temperature components of power generating plants. One of the applications of the ball-indentation technique is characterising the property gradients in the weld joints of these steels. Similarly mechanical property degradation of these steels due to aging at elevated temperatures can also be determined using ball-indentation technique[19]. If such an assessment is done without disturbing the structural integrity of the plant component and thereby minimizing the down time, then the economic benefits reaped are enormous.

5. CONCLUSION

The ball-indentation technique has been successfully benchmarked for determining the stress-strain properties of ferritic steels with different work hardening characteristics. The effects of pile-up have been incorporated in the analysis of ball-indentation data to accurately predict the tensile stress-strain properties. The constraint factors used for defining the representative stress and the constants used for defining the average strain matches well with the internationally reported values. Thus ball-indentation technique and the testing methodology adopted in this study have the potential to be applied insitu and non-destructively to evaluate the mechanical properties of small volumes such as welds, heat affected zones and aged components.

6. ACKNOWLEGEMENTS

The authors also thank Shri P.Kalyanasundaram, Associate Director, Inspection Technologies Group, Indira Gandhi Centre for Atomic Research, for his keen interest and encouragement in this work. The help of Shri M. Sekar during the course of work is duly acknowledged

REFERENCES

1. Tabor D, *The Hardness of Metals,* Clarendron Press, Oxford (1951).
2. Murty K L, Miraglia P Q, Mathew M D, Shah V N and Haggag F M, *International Journal of Pressure Vessels and piping*, **76** (1999) p 361.
3. Mathew M D, and Murty K L, Journal of Materials Science **34** (1999) p 1497.
4. Mathew M D, and Murty K L, "Condition Monitoring of structural materials using non-destructive ball-indentation technique", Proceedings of *International Symposium on Material Aging and Life Management (ISOMALM 2000)* **3** p 1386.
5. George. E. Dieter, *Mechanical Metallurgy*, SI Metric Edition, McGraw-Hill (UK) p 327.
6. Francis H A, *Transactions of ASME*, (1976) p 272.
7. Tirupataiah Y and Sundararjan G, *Metallurigical Transactions* A, **22A** (1991) p 2375.
8. Jeong-Hoon Ahn and Dongil Kwon, Journal *of Materials Research*, **16**(11) (2001) p 3170.
9. Sung-Hoon Kim, Min-Kyung Baik and Dongil Kwon, *Journal of Engineering Materials and Technology*, **127**(3) (2005) p 265.
10. George E. Dieter, *Mechanical Metallurgy*, SI Metric Edition, McGraw-Hill (UK) p 287.
11. Tirupataiah Y, *Journal of Materials Science and Engineering*, **91** (1987) p 169.
12. Au P, Lucas G E, Scheckerd J and Odette G R, *Non-Destructive Evaluation in Nuclear Industry*, American Society for Metals, Metal Park, OH, (1980) p 597.
13. Haggag F M, "*Small Specimen Test Techniques applied to Nuclear Reactor Vessel Thermal Annealing and Plant Life Extension*", (eds) W.R.Corwin, F.M.Haggag, and W.L.Server, ASTM STP **1204** (1993) p 27.
14. Sneddon I N, *International Journal of Engineering Science*, **3** (1965) p 47.
15. Norbury A L and Samuel T, Journal *of Iron Steel Institute*, **117** (1928) p 673.
16. Hill R, Storakers B and Zdunek A B, *Proceedings of Royal Society of London*, Ser A **423** (1989) p 301.
17. Kishore R and Sinha T.K, *Metallurgical and Materials Transactions A*, **27A**, (1996) p 3340.
18. Taljat B, Zacharia T and Kosel F, *Int Journal of Solids Structures*, **35**(33) (1998) p 4411.
19. Mathew M D, Murty K L, Rao K B S, and Mannan S L, *Material Science Engineering*, **A264** (1999) p159.